By acceptance of this article, the publisher or recipient acknowledges the U.S. Government's right to retain a nonexclusive, royalty-free license in and to any copyright covering the article.

Conf-810754--4

THE EFFECTS OF LOW-ENERGY-ELECTRON-CAPTURE COLLISIONS ($H_o + C^{n+}$) ON THE PARTICLE AND ENERGY BALANCE OF TOKAMAK PLASMAS*

CONF-810754--4

DE82 018263

John T. Hogan

Oak Ridge National Laboratory
Oak Ridge, Tennessee 37830

MASTER

*Research sponsored by the Office of Fusion Energy, U.S. Department of Energy, under contract W-7405-eng-26 with the Union Carbide Corporation.

DISCLAIMER

This report was prepared as an account of work sponsored by an agency of the United States Government. Neither the United States Government nor any agency thereof, nor any of their employees, makes any warranty, express or implied, or assumes any legal liability or responsibility for the accuracy, completeness, or usefulness of any information, apparatus, product, or process disclosed, or represents that its use would not infringe privately owned rights. Reference herein to any specific commercial product, process, or service by trade name, trademark, manufacturer, or otherwise, does not necessarily constitute or imply its endorsement, recommendation, or favoring by the United States Government or any agency thereof. The views and opinions of authors expressed herein do not necessarily state or reflect those of the United States Government or any agency thereof.

DISTRIBUTION OF THIS DOCUMENT IS UNLIMITED

THE EFFECTS OF LOW ENERGY ELECTRON CAPTURE COLLISIONS ($H_o + C^{n+}$) ON THE PARTICLE AND ENERGY BALANCE OF TOKAMAK PLASMAS

John T. Hogan

Oak Ridge National Laboratory
Fusion Energy Division
Oak Ridge, Tennessee
U.S.A.

1. INTRODUCTION

The particle and energy balance in magnetic fusion plasmas is a complex subject in which atomic and molecular collisions data often plays a determining role. Appreciation for the many processes involved may be gained from the Proceedings of the NATO Advanced Study Institute on Atomic and Molecular Processes in Controlled Fusion Research [1], from the published proceedings of the IAEA Advisory Committee Meetings on Atomic and Molecular Data for Fusion [2,3], and from a recent topical article on atomic physics processes in fusion [4].

To illustrate the way in which atomic data provides enlightenment in the search for understandable (and thus extrapolable) confinement models, we restrict our scope to electron capture collisions involving H_o and multiply-charged ions. Many such foreign (impurity) multiply-charged ion species are found in plasma discharges, as a result of gas recycling and damage to the surrounding surfaces by energetic plasma particles. Typical 'low-Z' ions are carbon and oxygen; the major constituents of the stainless steel wall (Fe, Ni, Cr) are intermediate impurities, while 'high-Z' impurities (Mo, W) enter from 'limiter' plates which constrict the hot plasma zone to reduce direct plasma-wall contact. In this discussion, however, attention will be given only to applications of data involving $H_o + C^{n+} \rightarrow H^+ + C^{(n-1)+}$ reactions with energy 10 eV to 2 keV. This energy range is typical of the plasma edge in present devices. The reasons for choosing only carbon for discussion are:

a) As a result of recent theoretical and experimental progress, some reported at this conference, the electron capture rates for the full suite of charge states ($C^{2+} \rightarrow C^{6+}$) of interest in the plasma edge may be estimated for the first time.

b) Electron impact ionization cross-sections have been measured for these ions, and the use of semi-empirical ionization rates is supported by direct measurement [5,6].

c) The cross-sections for electron capture have been found to be sufficiently large that, taken together with the typical measured H^o concentrations in the edge region, this process is the dominant recombination mechanism for C^{n+} by a wide margin: hence both the dominant ionization and recombination processes may be estimated for the full suite of C^{n+} ions of interest.

d) This situation does not exist for any other impurity ion of fusion interest: a need exists for data in this energy range for impurity ions found in fusion plasmas.

While it is encouraging to be able to make quantitative estimates for a particular process for the first time, it is not necessarily true <u>a priori</u> that the results

will be relevant to fusion. In this case, however, the results have a major impact in several topical areas:

a) An attempt is being made to fashion a 'photosphere,' [7] or 'cool plasma mantle' [8] around future large fusion plasmas. It would be desirable to create, and maintain, a radiating zone on the plasma periphery in which power deposited in the plasma core by thermalizing α-particle reaction products is lost to low-Z impurity ions and then radiated from the plasma. Wall damage (and subsequent introduction of a large number of impurities) would thus be minimized. Since $H_o + H^+$ charge exchange in the edge region creates an efflux of energetic neutral atoms which can sputter wall atoms into the discharge, it is desired to keep the temperature of the radiative zone well below the maximum in the sputtering yield. (As a typical value, S_{max} occurs at ∿2 keV for F_e.) Thus, we will adopt 350 eV as the upper limit of our temperature range.

b) Recent high-power heating results have been carried out with graphite limiters. The dominant impurity ion in these cases is carbon, and the contribution of carbon radiation to the overall energy balance is significant [9].

c) Study of the dynamics of impurity motion has disclosed asymmetries in the emitted light, which could confound collisional (so-called 'neoclassical') theory. While a theoretical analysis predicts small asymmetries to result from the theory, quite large asymmetries are measured. The possible role of charge-exchange of H_o with multi-charged impurities in producing this asymmetry has been suggested [10], but the lack of data has prevented calculation till now.

2. ATOMIC DATA USED IN THE CALCULATIONS

Calculation of the impurity charge state and radiative cooling power requires the solution of the ionization-recombination balance equations for multiply-charged ions in a plasma with specified temperature and density. These calculations are routine, and the usual estimates for <Z> (charge state) and P_{RAD} (radiative cooling power) are available in tabular form [11]. However, these conventional estimates cannot be used for the plasma edge, because charge exchange recombination has not been included in them. Hence we recompute the so-called coronal equilibrium relative abundances and radiative cooling rates for typical plasma conditions.

2.1 Balance Equations

The steady-state equations for the ionization-recombination balance are:

$$0 = I^i_{k-1} n^i_{k-1} + R^i_{k+1} n^i_{k+1} - (I^i_k + R^i_k) n^i_k \qquad (1)$$

I_k, R_k are the total ionization rates for the ion with charge $Z_k = k - 1$ ($k = 1, \ldots, Z$); n^i_k is the spatial density of that ion; i denotes the spatial zone.

Plasma transport has a large effect on radiation and in the diagnostic applications of spectroscopic data [12]. Because the calculation of cooling rates without including transport processes, but comparing cases with and without charge exchange recombination, will give a fair picture of the changes made when the new data are taken into account we will neglect plasma transport processes.

2.2 Ionization and radiative and dielectronic recombination rates

Restricting attention to the case of carbon, we use the semi-empirical Lotz formulae to calculate the electron impact ionization rates [5]. The justification for using this rate has been presented by Crandall [6]. Uncertainties of up to 40% with respect to the data we use are suggested, and so the sensitivity of our results to variation in this rate is examined in Section 6. The total recombination rate for plasmas in the density and temperature range we consider has contributions from radiative, dielectronic, and charge exchange-induced recombination. The expressions which we use for radiative and dielectronic recombination have been described by Mattioli [13]. They embody estimates by Von Goeler et al. [14] for radiative recombination and the results of Burgess [15] are used for the dielectronic recombination rate. Again, the sensitivity to variations in the assumed data is treated in Section 6.

2.3 Charge-exchange Induced Recombination

The rate of recombination due to electron capture reactions is

$$\alpha_{cx}^{Z} = n_o n_Z \sigma_{cx}^{Z} V_{th}(H_o)$$

where σ_{cx}^{Z} is the cross-section for electron capture from H_o, n_o is the neutral hydrogen density, and $V_{th}(H_o)$ is the hydrogen thermal speed. In Monte Carlo calculations of n_o, the exact particle thermal speed is used. However, for steady state radiative cooling calculations we assume $V_{th}(H_o)$ is equal to the hydrogen ion thermal speed, and that $T_e = T_i$. Low T_e in the plasma edge, and the good electron-proton energy coupling which this implies, serves to justify this simplification.

The atomic data used for σ_{cx}^{Z} are as follows: Theoretical values for C^{2+}, C^{3+} (electron capture to C^{+}, C^{2+}, respectively) have been obtained by Heil and Bottcher [16] extending previous results of Heil, Dalgarno and Butler [17], for energies up to ∿250 eV/amu. Experimental results for C^{2+} electron capture [18] are used for energies above 500 eV/amu, and (approximately coincident) theoretical and experimental [19] results are used for C^{3+} for all energies considered.

Theoretical results for $C^{4+,5+}$ presented by Olson, Shipsey, and Browne [20,21] are assumed. Other theoretical work [22] and recent experiments [19] suggest that factor 2 variations about these values should be studied. The sensitivity of the results to these uncertainties will be discussed in Section 6.

2.4 Discussion

The most significant aspect of the cross-section data for charge exchange is the large difference between the C^{3+} and C^{4+} cross sections. C^{4+} will readily recombine to C^{3+}, but there will be a sharply reduced flow from C^{3+} downwards. The relative population of this strongly radiating Li-like ion will thereby be enhanced by charge exchange effects.

The existence of a large C^{6+} cross-section implies that fully stripped carbon will only be found in plasmas at much higher electron temperatures than heretofore calculated.

3. PARTICLE BALANCE: NEUTRAL DENSITY

3.1 Particle Balance

The particle balance in the plasma may be viewed as a form of book-keeping, to ensure that sources and losses of particles add up to the observed rate of change of density. Balance equations for particles are given in Ref. [1]. The source of particles due to impurity stripping, from beam injection, and from ionization of neutral hydrogen atoms must be computed; hence neutral gas transport should be calculated.

3.2 Neutral Transport

Charge exchange processes can influence the spatial distribution of H_o in the plasma (and thus the particle balance through the source term). Neutral particles travel freely, of course, with respect to the magnetic field. Their transport is governed by the Boltzmann equation, with impact ionization and (resonant) $H_o + H^+$ charge exchange the dominant atomic collisions effects which must be considered. The transport equation is described, e.g., in [23].

The transport of neutrals is affected by electron impact ionization (annihilation) by the exchange of velocities with the background hydrogenic ion population, and by annihilation of the neutral by $H_o + C^{n+}$ electron capture. Although the electron capture cross sections for H_o with multiply charged ions are larger than that for $e^- + H_o$ impact ionization, the much larger electron thermal speed leads to the domination of impact ionization over the impurity charge exchange process as an annihilation mechanism for many cases of interest.

Neutral densities in the plasma edge in the range 10^{10}-10^{11} cm^{-3} are typically estimated. However, the asymmetric nature of the spatial distribution of external sources of neutrals can lead to much higher local densities. The sources are cold neutrals injected for fueling, (1-10 eV); Franck-Condon dissociative ionization of H_2^o on the walls of the device, diffusing there from the bulk metal (1-10 eV) [24]; ions, neutralized at the limiter, and re-entering with energies typical of plasma on the outermost flux surface (10 eV ∿ 100 eV); and emergent charge exchange neutrals reflected from the wall with intermediate energies close to ion energies in the plasma edge (100 eV ∿ 2 keV).

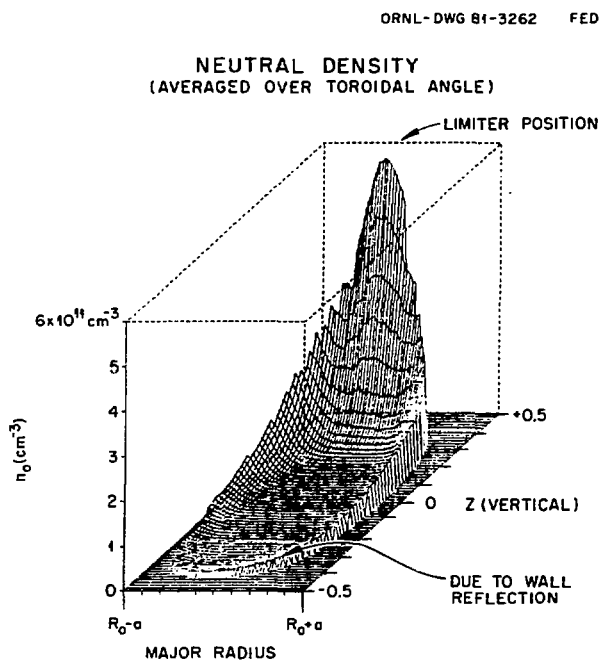

Figure 1
Spatial density of H_o: $n_o(r,\phi,Z)$ (ϕ the toroidal angle) is averaged with respect to ϕ and shown as a function of major toroidal radius, r, and the vertical dimension, Z. The source of particles in this Monte Carlo calculation is assumed to be the top center of the box: this is typical of emission from a horizontal rail limiter. Parameters are chosen to be typical of an

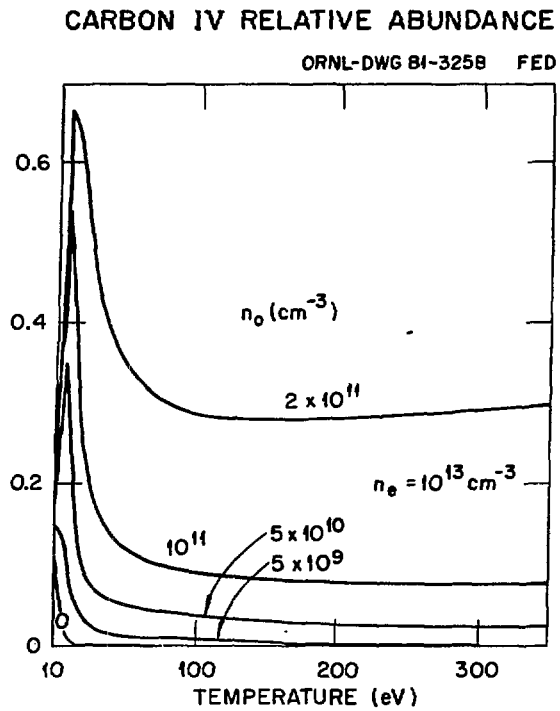

2a

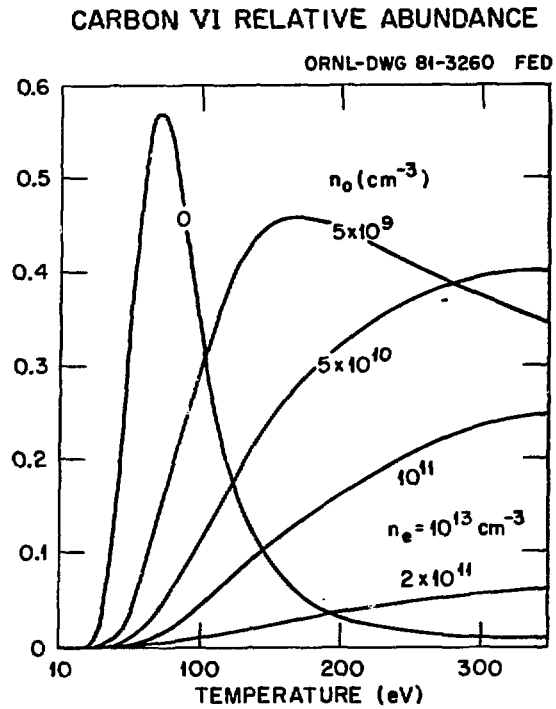

2c

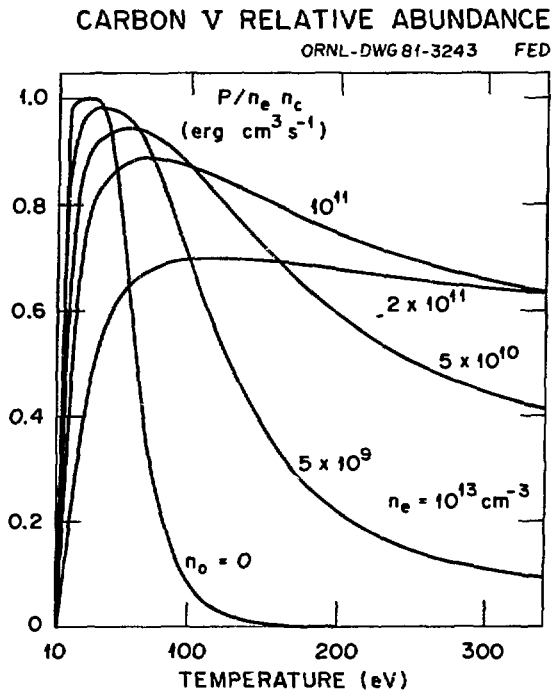

2b

Figure 2
The relative abundance of CIV, CV and CVI ions with respect to the total carbon density. In these, as in all subsequent figures showing neutral density effects (i.e., Figures 3, 4, 5 and 7) the values displayed are valid for other cases with the same ratio of n_o/n_e. Here $n_e = 10^{13}$ cm^{-3} has been chosen for specificity, hence the results displayed for $n_o = 2\text{-}10^{11}$ cm^{-3}, say, are also true for $n_o = 10^{11}$ cm^{-3}, $n_e = 5\text{-}10^{12}$ cm^{-3}. The temperature range is 10 eV to 350 eV.

a. relative abundance of CIV
b. relative abundance of CV
c. relative abundance of CVI

Two of the sources mentioned are strongly localized in space: gas injection (commonly called 'puffing') and limiter recycling. Figure 1 shows a typical calculated distribution of neutral hydrogen density around the cross section of the torus. Gas is assumed to enter from a rail limiter, near the top of the cross-section. Particles are then followed with a 3-dimensional Monte Carlo code, which includes the processes needed for the Boltzmann equation description [25].

The code assumes that plasma parameters (density, temperature, e.g.) are constant on magnetic flux surfaces, because of the rapid communication around flux surfaces due to motion along field lines.

3.3 DISCUSSION

As seen in Fig. 1 there may be a factor of 3-5 difference between local values of the neutral density and the flux surface average (which enters the particle balance). The local density, of course, must be used for calculations of radiative cooling enhancement and charge state depression due to charge exchange with impurities. However, this lack of symmetry is an expected effect arising from the spatial localization of the neutral particle source and the straight-line flight of the neutral atoms.

4. RELATIVE ABUNDANCES AND RADIATIVE COOLING RATES

4.1 Relative Abundance

The ratio of the number of ions with charge Z to the total number of carbon ions at a spatial location is computed from the steady-state balance equation. The results for $C^{3+} \rightarrow C^{5+}$ are shown in Figure 2a-c. Several features of fusion interest emerge.

The coronal equilibrium dependence of relative abundance solely on T_e is destroyed with the correct treatment of C^{n+} charge exchange. For $\sigma^Z_{cx} = 0$, there is a sharp localization of relative abundance with respect to temperature (as seen in the $n_o = 0$ cases in Figures 2a-c). The existence of a peak in, e.g., CV emission in the plasma, has in the past been used to give the temperature value at that position. This diagnostic application is only possible, however, when the ratio n_o/n_e is less than $\sim 2\text{-}10^{-4}$. This can be a stringent requirement during high-power heating experiments when intense 'gas puffing' is used to fuel the discharge.

The most apparent effect of the charge exchange reactions is to depress the average charge of the carbon at a given temperature. As seen in Figure 3, with $n_o = 0$ (or, equivalently $\sigma^Z_{cx} = 0$) the $\langle Z \rangle \equiv \Sigma Z_k n_k / \Sigma n_k$ quickly rises to the fully ionized value above a temperature of $\sim$100 eV. With $\sigma^Z_{cx} \neq 0$, however, the fully stripped stage is not attained in the 10-350 eV temperature range of interest for plasma edge calculations.

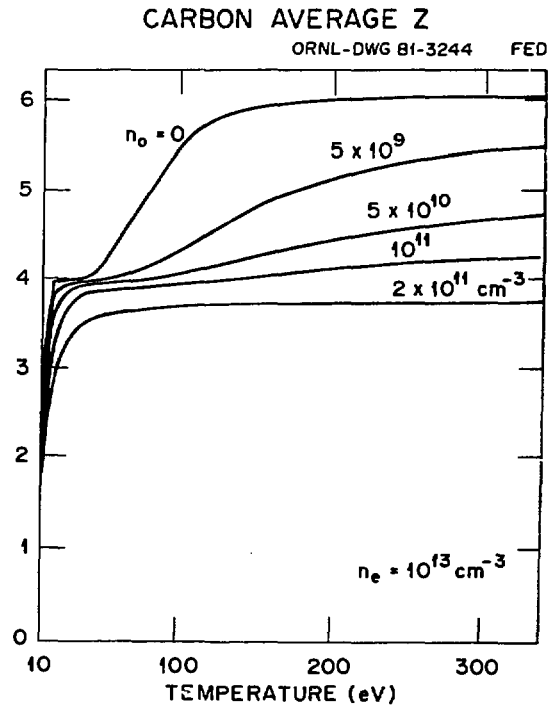

Figure 3
The average ionic charge of carbon ions for T_e = 10-350 eV, $n_o = 0\text{-}2.10^{11}$ cm^{-3}

4.2 Radiative Cooling Rates

The calculation of radiative emission can proceed once all the relative abundances have been found. We include contributions to radiation arising from radiative and dielectronic recombination, and from line radiation, using estimates calculated by Breton et al [26,27]. The major effect of charge exchange collisions is to enhance the recombination rate, and hence to increase the abundance of radiating ions. The electron energy added to the plasma with H_o, transferred to excited states of C^{n+} and subsequently radiated is not counted as a direct cooling loss from the plasma electrons.

Typical results, indicating both the relative contributions of radiative and dielectronic recombination, and line radiation losses are shown in Figures 4a-c. We have chosen CV as a typical ion spectroscopically observed in the plasma edge. The cooling rates are expressed as power per electron per CV ion. The total radiative and dielectronic recombination rate, shown in Figure 4a, has a peak value of $\sim 2.10^{-21}$ erg cm^3 s^{-1}, while the line radiation has a peak some 40 times higher. For both, though, there is a very large enhancement due to charge exchange recombination. The total CV radiation, shown in Figure 4c, peaks at $\sim$70 eV with a charge exchange, but with $\sigma^Z_{cx} \neq 0$ the radiative cooling rate rise throughout the plasma edge energy range.

For application to 'cool plasma mantle', or 'photosphere' techniques the total carbon radiation is of interest. This is shown for the relevant energy range in Figure 5. If 'mantle' temperatures can be kept in the 10-20 eV range, then radiative rates of 2-3 W/cm^3 can be achieved for an electron density of 10^{13} cm^{-3} and a carbon density 2.10^{12} cm^{-3}. This cooling rate could radiate most of the power emission in the presently considered design for the Fusion Engineering Device [28], with a radiating layer only $\sim$10 cm thick, as compared with the plasma minor radius of 125 cm. (The goals of the FED are to produce sufficient thermonuclear power to demonstrate the engineering features of a fusion power plant: neutron shielding, tritium breeding, blanket, etc.). As the temperature is increased, the width of the radiating layer would have to be increased as well.

The discrepancy between the rate calculated including charge exchange, and that without, is approximately two orders of magnitude at T_e = 100 eV!

5. IMPURITY DYNAMICS

An important experimental finding, related to the validity of neoclassical theory, has been the observation of spatial asymmetry in impurity light emission [10,29, 30]. The assumption that plasma parameters should be approximately constant on magnetic flux surfaces, and hence symmetric in space, is a typical assumption in theoretical models. Corrections to the collisional diffusion theory have been proposed [31], but the maximum asymmetry allowed is approximately 25%. Much larger discrepancies (typically a factor 2 variation in light emission) are observed.

The asymmetry in the neutral hydrogen distribution, discussed in Section 3, yields a natural explanation for the observations. The predicted spatial distribution of CV is shown in Figure 6a, with $\sigma^Z_{cx} = 0$ assumed. Figure 6b shows the case for $\sigma^Z_{cx} \neq 0$, with only the left half of the CV spatial distribution ($\phi < \Pi$) presented for clarity. The distribution is symmetric about the $\phi = \Pi$ plane, and shows a pronounced dip where the neutral hydrogen density has a peak near the limiter. This model thus traces the asymmetry in impurity light emission to the naturally asymmetric H_o spatial distribution. The spatial localization of the H_o distribution (and hence of carbon light emission) will depend on the details of placement of the limiter and gas injection parts for specific experiments.

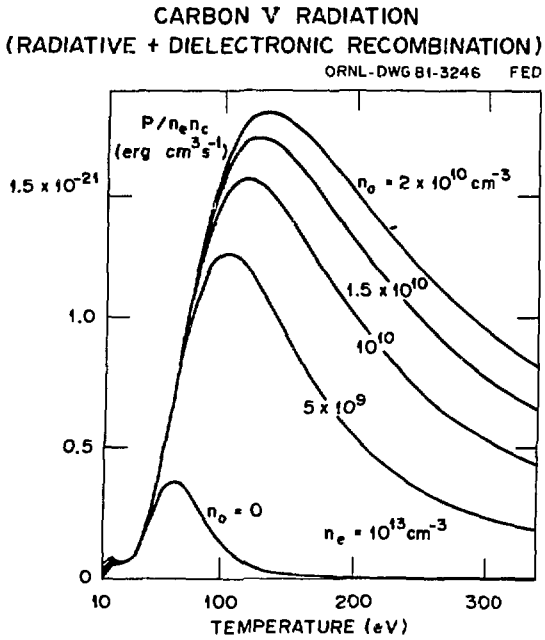

4a

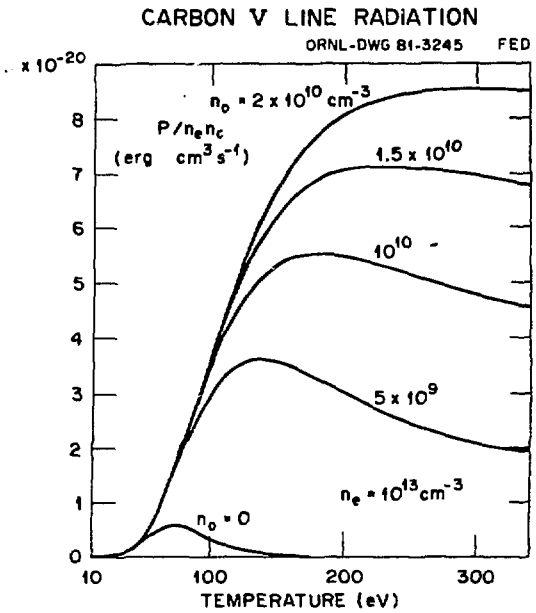

4c

Figure 4
Radiative rates for CV ions, for T_e = 10-350 eV, n_o = 0-2.10^{11} cm^{-3}.

a. The contributions from radiative and dielectronic recombination events.
b. Total line radiation emission.
c. The overall radiative rate, summing contributions in 4b and 4c.

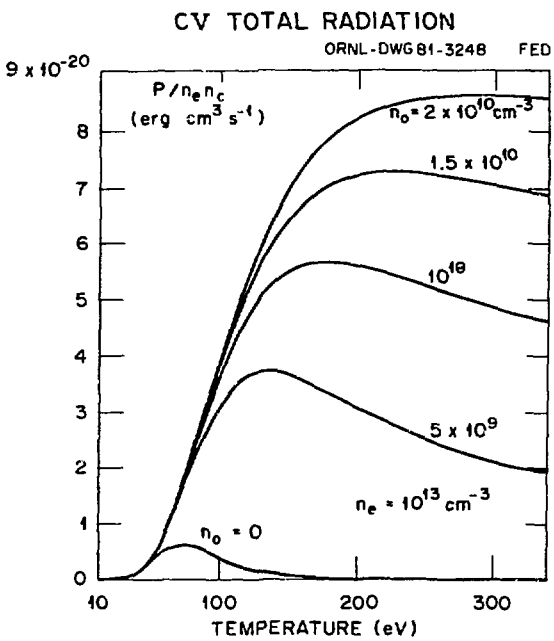

4b

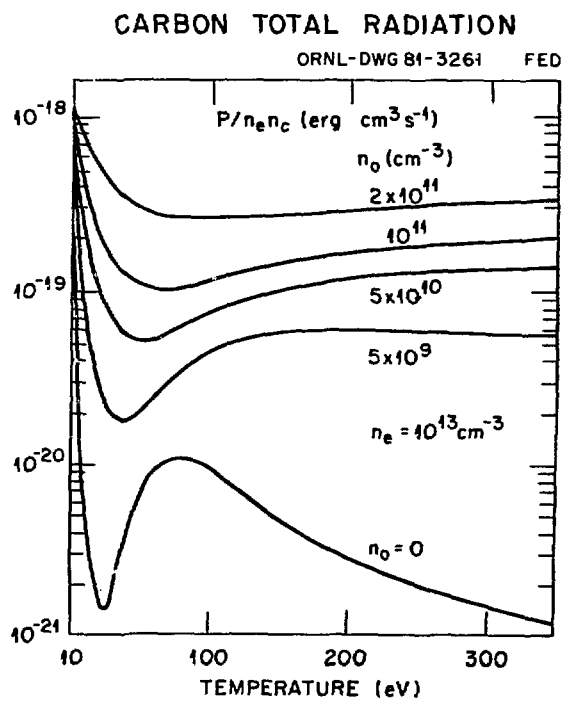

Figure 5
Total radiative cooling for all carbon ions, for T_e = 10-350 eV, n_o = 0-2.10^{11} cm^{-3}. Results are expressed as the power radiated per electron per carbon ion.

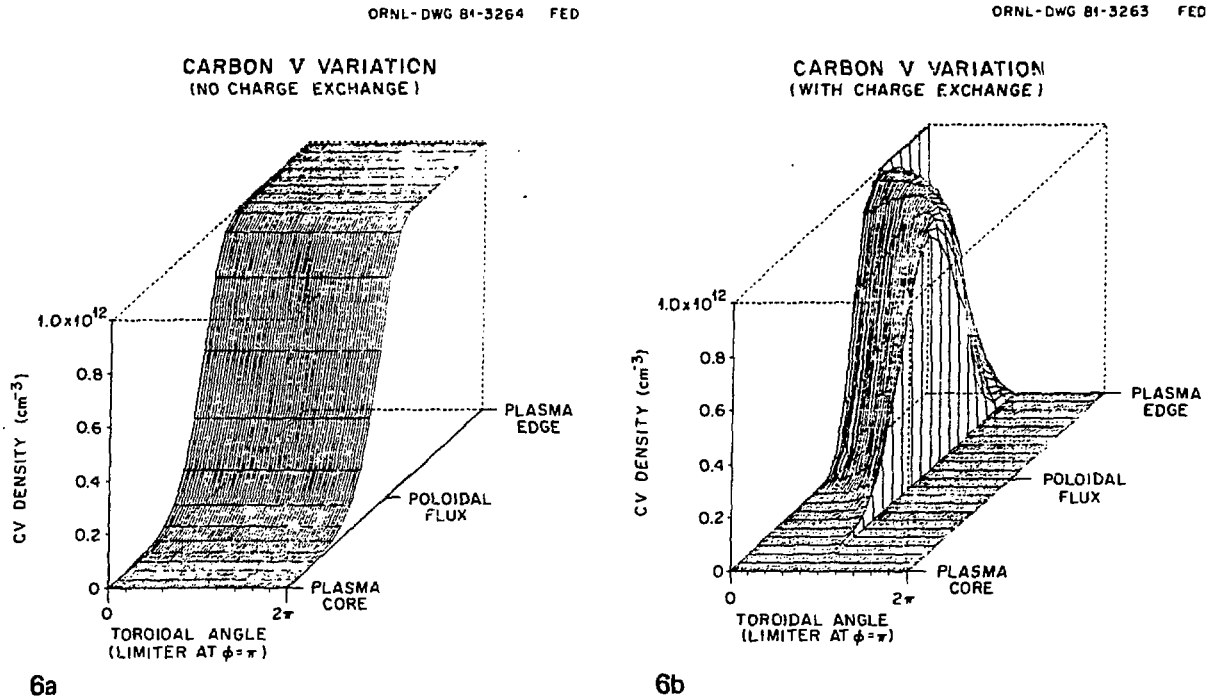

Figure 6

Effects of charge transfer between H_0 and multiply charged carbon impurities on the spatial distribution of a typical carbon ion, CV. The results are shown as functions of the angle around the torus (with particles entering the plasma at $\phi = \Pi$), and of the poloidal magnetic flux, which serves to label surfaces with constant plasma density, temperature, etc.

a. $\sigma^Z_{cx} = 0$ assumed, the CV relative abundance depends only on T_e, hence it is depressed in the plasma core (T_e = 700 eV) and rises toward the plasma edge (T_e = 50 eV). No dependence on ϕ is present since T_e depends only on the value of poloidal magnetic flux, which does not change as ϕ changes.

b. Same conditions as in 6a, but now the correct cross-sections for σ^Z_{cx} are included. The CV distribution is strongly asymmetric. For clarity in viewing, the right half of the CV distribution has been excised in this Figure ($\phi > \Pi$). The computed distribution is mirror-symmetric about $\phi = \Pi$.

6. SENSITIVITY ANALYSIS

The atomic data which have been used for these calculations are susceptible to improvements in accuracy. The specific needs discussed here, which bear on obtaining an accurate particle and energy balance for some magnetically confined plasmas, are met by the available data. Improvements would be welcome for diagnostic purposes, and the details of 'cool plasma mantle', or 'photosphere', power emission scheme will require a narrower range for some cross-sections. To discuss the accuracy of the data, we compute the sensitivity of the results to variations in the assumed atomic data. The reference values used are those described in Section 2.

6.1 Electron Impact Ionization

The uncertainty in using the Lotz semi-empirical ionization rates is often quoted as 40%. We have found that the variation in total radiated power produced by

enhancing the Lotz rate by a factor 1-1.4 is a decrease by 30% in the 30 eV region, and there is a smaller decrease elsewhere.

6.2 Radiative and Dielectronic Recombination

The carbon charge exchange rate is the dominant recombination process, hence there is only a small sensitivity to variation of the dielectronic and radiative recombination rates. Figure 7a shows the results of a 1-400X enhancement of the dielectronic recombination rate on the radiated power. A significant difference is seen only where the Li-like ion is active (T_e < 50 eV) and these by a factor 2. The same variation in the radiative recombination rate produces an order of magnitude smaller change.

6.3 Charge Exchange Cross-sections

The cross-sections for C^{3+}, C^{4+}, and C^{5+} collisions have been measured over much of our relevant energy range and are typically within a factor 2 of theoretical calculations. Using the base data described in Section 2, then, we study the sensitivity in the radiative cooling rate to changes in the $C^{3+,4+,5+}$ cross-sections, and the C^{6+} cross-sections separately. Since the C^{6+} cross-sections has not been measured over the whole energy range, the results of the parameters variation are somewhat more critical.

For the $C^{3+,4+,5+}$ variation (Figure 7b) the uncertainty in cross-section strongly affects the variation in the cooling rate. Hence, while the general features of the cooling rate curves are similar, if the cross-sections were to be a factor 2 lower than the center of the present experimental range, then a larger portion of the edge plasma would be needed to provide the required radiative emissions.

For C^{6+} the sensitivity has been found to be smaller since the lower ionization stages radiate more effectively. The presence of significant radiation levels at high temperature is maintained (Fig. 7c).

7. DISCUSSION

The particle and energy balance in magnetically confined fusion plasmas must inevitably be affected by atomic collisions processes, if only because perfect isolation from material surfaces is impossible. The particular process considered here, $H_o + C^{n+}$ electron capture reactions in the 10 eV - 2 keV plasma edge thermal range, illustrates the typical role of collisions data in magnetic fusion particle and energy balance.

The inclusion of charge exchange cross-section data for the suite of carbon ions expected at these temperatures produces the following results:

- The dependence of relative abundance on T_e, characteristic of steady-state conditions without significant neutral hydrogen density ($n_o/n_e < 2.10^{-4}$) is replaced by a dependence on n_o and T_e. Further, the localization of relative abundance in a narrow temperature range is lost. Incompletely stripped carbon ions will exist, for typical neutral densities, at temperatures above 300 eV.

- Radiative cooling rates are enhanced by several orders of magnitude over those calculated with $\sigma^Z_{cx} = 0$. The levels are sufficient to encourage further attempts to fashion a radiative layer for transmission of large fusion power fluxes to external surfaces in future reactors. The large difference between charge exchange

cross-sections for C^{4+} and C^{3+} leads to efficiently radiating charge states being well populated.

• Spatial asymmetries in light emission, viewed as a possible paradox with regard to drift-collision theory, are seen as a natural consequence of the asymmetry of the neutral hydrogen spatial distribution and the large values of the charge exchange cross-sections for C^{4+}, C^{5+}.

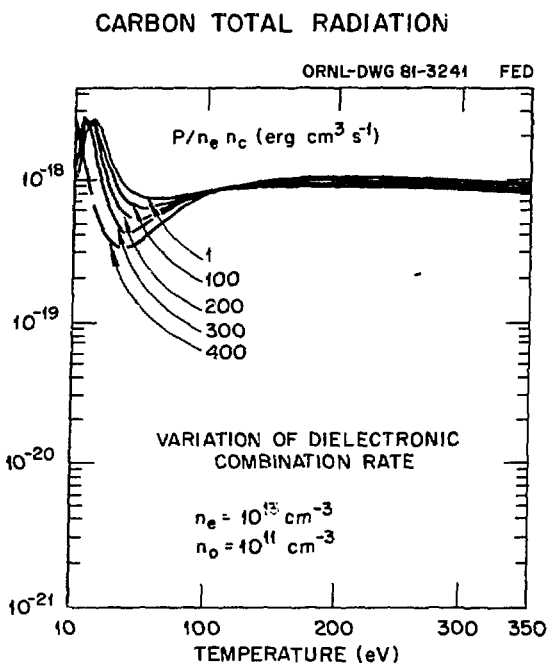

7a

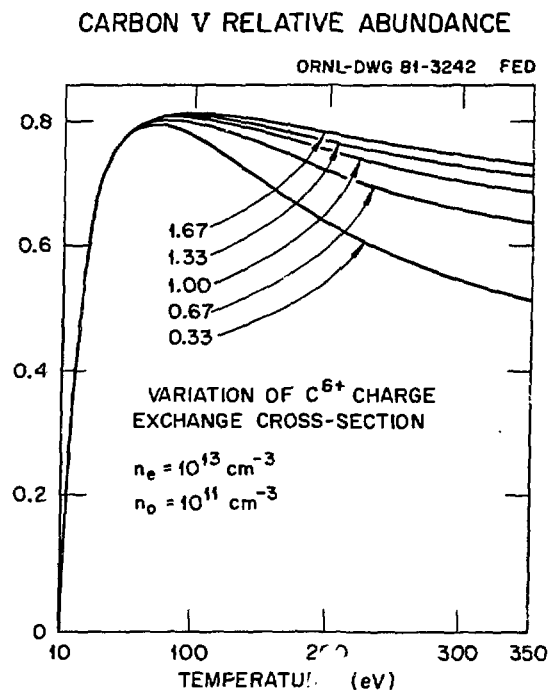

7c

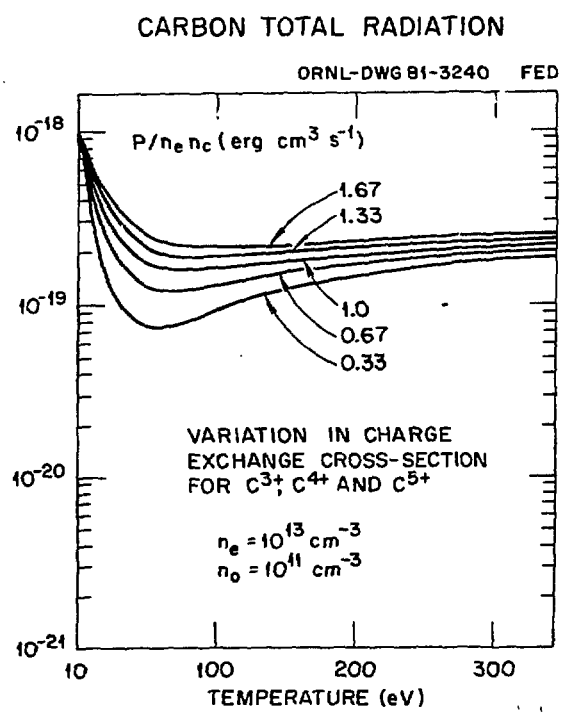

Figure 7
Sensitivity to variations in atomic data. For these cases $n_o/n_e = 10^{-2}$ has been assumed ($n_o = 10^{11}$ cm^{-3}, $n_e = 10^{13}$ cm^{-3}). T_e = 10 eV - 350 eV.

a. Variation of the dielectronic recombination rate. Cases for 1-400X the reference rate are shown.

b. Variation in the base cross-section for C^{3+}, C^{4+}, C^{5+} + H_o reactions (0.33-1.67X).

c. Variation in the C^{6+} + H_o cross-section (0.33 → 1.67 X).

REFERENCES

[1] Atomic and Molecular Processes in Controlled Thermonuclear Fusion, NATO Advanced Study Institutes, Series B: Physics, Vol. 53 (Eds., M.R.C. McDowell, A. M. Ferendici) Plenum Press, New York, 1980.

[2] Proceedings of the IAEA Advisory Group Meeting on Atomic and Molecular Data for Fusion, held at Culham Laboratory (UKAEA) 1976. Proceedings published by IAEA, Vienna, as IAEA-199 (1977). Invited papers published in Physics Reports, J. Phys. 37C (1978).

[3] Proceedings of the Second IAEA Advisory Group Meeting on Atomic and Molecular Data for fusion, held at CEN/Fontenay-aux-Roses Laboratory (CEA) 1979. Invited papers published in Physica Scripta 23 (1981).

[4] K. Dolder, J. Hogan, Comments on Plasma Physics and Controlled Fusion, 6 1 (1980).

[5] W. Lotz, Z. Phys. 216 241 (1968), Z. Phys. 220 466 (1969).

[6] D. H. Crandall, Physica Scripta 23 154 (1981).

[7] K. Lackner, private communication.

[8] A. Gibson, M. Watkins, Proc. 8th European Conference on Controlled Nuclear Fusion and Plasma Physics, Prague, 1977, Vol. I, p. 31.

[9] PLT Group, Proc. 7th International Conference on Plasma Physics and Controlled Nuclear Fusion, Innsbruck, 1978, IAEA Vienna 1 (167) 1979.

[10] S. L. Allen, H. W. Moos, R. K. Richards, J. L. Terry, E. S. Marmar, Nuclear Fusion 21 (251) 1981.

[11] R. V. Jensen, D. E. Post, C. B. Tarter, W. H. Grasberger, W. A. Lokke, Atomic and Nuclear Data Tables 20 397 (1977).

[12] S. Suckewer, E. Hinnov, M. Bitter, R. Hulse, D. Post, Phys. Rev. A 22 725 (1980).

[13] M. Mattioli CEN/Fontenay-aux-Roses Report EUR-CEA-FC 761 (1975).

[14] S. Von Goeler, W. Stodiek, H. Eubank, H. Fishman, S. Grebenshikov, E. Hinnov, Nucl. Fusion 15 301 (1975).

[15] A. Burgess, Astrophys. Jour. 141 1588 (1965).

[16] T. Heil, C. Bottcher, Proc. XII ICPEAC and private communication.

[17] T. Heil, A. Dalgarno, J. Phys. B. Lett. 12 L557 (1979); S. E. Butler, Phys. Rev. A 20 2317 (1979).

[18] W. L. Nutt, R. W. McCullough, H. B. Gilbody, J. Phys. B Letters 11 L181 (1978).

[19] R. Phaneuf., Phys. Rev. A. 24 1138 (1981).

[20] R. E. Olson, E. J. Shipsey, J. C. Browne, J. Phys. B 11, 699 (1978).

[21] E. J. Shipsey, J. C. Browne, R. E. Olson, J. Phys. B. 14 869 (1981).

[22] M. Gargand, H. Hassen, R. McCarroll, P. Valiron, Proc. XII ICPEAC.

[23] J. T. Hogan, Methods in Computational Phys., V. 16, Applications to Controlled Fusion Research, ch. 3, (B. Alder, S. Fernbach, J. Killeen, eds.) Academic Press, New York, 1976.

[24] H. C. Howe, J. Nucl. Materials 93 and 94 17 (1980).

[25] G. G. Kelley (private communication).

[26] C. Breton, C. DeMichelis, M. Mattioli, Nucl. Fusion 16 891 (1976).

[27] C. Breton, C. DeMichelis, M. Mattioli, Nucl. Fusion CEN/Fontenay-aux-Roses Report EUR-CEA-FC 853 (1976).

[28] C. A. Flanagan, D. Steiner, G. E. Smith and the FED Design Center Staff, Oak Ridge National Laboratory Report ORNL/TM-7777, June 1981.

[29] S. Suckewer, E. Hinnov, J. Schivell, Bull. Amer. Phys. Soc. 23 697 (1978), also Princeton Plasma Physics Laboratory Report PPPL1430 (March 1978).

[30] J. L. Terry, E. S. Marmar, K. I. Chen, H. W. Moos, Phys. Rev. Lett. 39 1615 (1977).

[31] K. H. Burrell, S. K. Wong, Nucl. Fusion 19 1571 (1979).